Spatial Characterization of a Large-Format, Fine-Pitch CdZnTe Pixel Detector for the HEFT Balloon-Borne Experiment

C. M. Hubert Chen, Walter R. Cook, Fiona A. Harrison and Jiao Y. Y. Lin

***Abstract*— We have developed a large-format CdZnTe pixel detector with custom, low-noise ASIC readout, for astrophysical applications. In particular, this detector is targeted for use in the High Energy Focusing Telescope (HEFT), a balloon-borne experiment with focusing optics for 20–70 keV. The detector is a 24x44 pixel array of 498-micrometre pitch. As a focal plane detector, uniformity from pixel to pixel is much desirable. In this paper, we present the spatial characterization of some detector properties for the 1056 pixels on the HEFT detector. These properties include electronic noise, leakage current, spectral resolution and count rate.**

***Index Terms*— CdZnTe radiation detectors, radiation detector circuits, X-ray astronomy detectors.**

I. Introduction

We are developing cadmium zinc telluride (CdZnTe) *pixel* detectors for use on the focal planes of *focusing* telescopes. Specifically, the detector design that we present here is targeted for use in the High Energy Focusing Telescope[1], HEFT, which is a balloon-borne, hard-X-ray telescope, and for the future satellite mission, Constellation-X, in its hard X-ray telescope[2]. For HEFT, the detector needs to oversample a one-arcminute half-power diameter spot, and at the same time, cover a field of view of ten arcminutes or more. For a focal length of 6 m on HEFT, these dimensions translate to a spot size of 1.75 mm and a field of view of at least 17.5 mm. Our project emphasizes on getting good energy resolution from the detectors in the energy range 20–70 keV. In contrast, properties such as high count rate is not important in our application, as we shall only be looking at faint astronomical sources with HEFT.

As a focal plane detector, each HEFT detector contains over a thousand pixels, with each pixel having its own amplifier circuitry. The output of these pixels combine to form an image; thus, uniformity is desirable in the many properties of each pixel. To address this topic, we present the spatial characterization of some properties of the HEFT detector in this paper.

Manuscript received October 29, 2003. This research was supported by the NASA Space Science "Supporting Research and Technology" (SR&T) programme under Grant Number NAG5-5398. FAH was further supported by a Presidential Early Career Award, Grant Number NAG5-5322. JL was supported by the National Science Foundation under Grant Number DMR-020-4920.

All four authors are with the California Institute of Technology, Mail Code 220-47, Pasadena, CA 91125, USA. Email: hubert@srl.caltech.edu.

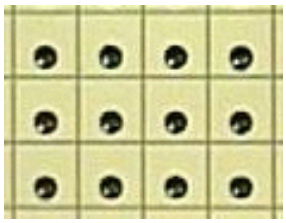

Fig. 2. The anode plane pattern, showing the 30-μm gaps between contacts, and the stencil-printed conductive epoxy bumps prior to bonding with the ASIC chip. The bumps are intentionally offset from the centre of the contacts. The pixel pitch is 498 μm.

II. Detector Configuration

The HEFT detector system consists of a CdZnTe-ASIC hybrid detector, an analog-to-digital converter (ADC) for the ASIC output, a microprocessor to operate the ASIC, and support electronics. Figure 1 is a schematic diagramme of a HEFT detector. We refer the readers to our earlier paper [3] for a description of the configuration of the system in more details. In the following, we concentrate on the CdZnTe and ASIC, which are relevant to the experiments described here.

A. CdZnTe

We purchase CdZnTe crystals with platinum electrodes from eV Products. The size of the sensor is 23.6 mm by 12.9 mm by 2 mm thick. This was the maximum size available given specification of single-crystal, highly uniform material at the time of our first design. The cathode is a monolithic platinum contact, while the anode plane is patterned into a 24×44 pixel array of 498-μm pitch, surrounded by a guard ring that is 1 mm on three sides, and 0.1 mm on the fourth (so that two detectors can be placed side by side to form a roughly square sensor area with minimal dead area in between). The gaps of bare CdZnTe surfaces in between anode contacts are 30 micrometres in width. Figure 2 shows the anode plane pattern at a few pixels.

B. Interconnect

The connection between each CdZnTe anode contact to the input of its read-out circuitry on the ASIC is made by flip-chip bonding. Each bond is a series connection of conductive epoxy bumps (on the CdZnTe) and gold stud bumps (on the ASIC).

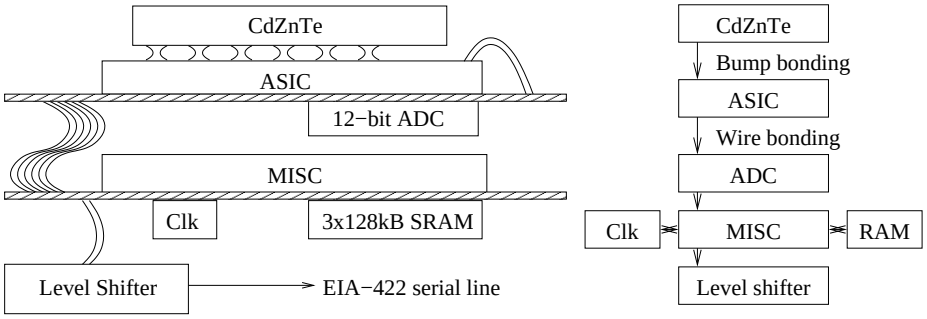

Fig. 1. Schematic diagramme of a HEFT detector.

These connections are about 40 μm tall. Four dots of RTV at the corners of the hybrid detector help to hold the CdZnTe and ASIC together, and no underfill material is used. More information on these interconnects is presented in Clayton et al [4] in these same proceedings.

C. ASIC Read-Out

We developed the custom ASIC at Caltech as part of the HEFT programme. It consists of a 24×44 pixel array, also of 498-μm pitch, with the pixel pattern matching that on the CdZnTe anode plane. Each pixel is implemented with its own preamplifier, shaping amplifier, discriminator, and sampling and pulsing circuits. All pixels share a serial readout line. We designed the ASIC for low noise and power; it consumes about 50 mW of power under normal operation. In order to achieve low power, we have chosen a design that is different from the conventional amplifier chain. In our design, the signal shaping and peak detection stages of the conventional chain are replaced by a bank of 16 switch capacitors arranged to continuously capture successive samples of the preamplifier output. The result is a large reduction in power dissipation—from 250 μW to 50 μW per pixel—while allowing off-chip digital signal processing to extract near optimal energy resolution. The implementation of the sample and store mechanism with a bank of 16 capacitors is illustrated in Fig. 3. The preamplifer output is converted to a current and is integrated by the capacitors, cyclically one by one, with a 1 μs integration time. This process gives us a record of the current level during the previous 15–16 μs at any given time. When a trigger is detected, sampling continues for 8 more samples, after which the circuit freezes while the samples are read out.

III. Spatial Characterization

In this section, we present the results we have obtained to date from the spatial characterization of our first detector of this design.

A. Electronic Noise

We measure the eletronic noise by sending pulser signals to each pixel which simulate a 75-keV spectral line. We assess the electronic noise as the linewidth of the pulser line.

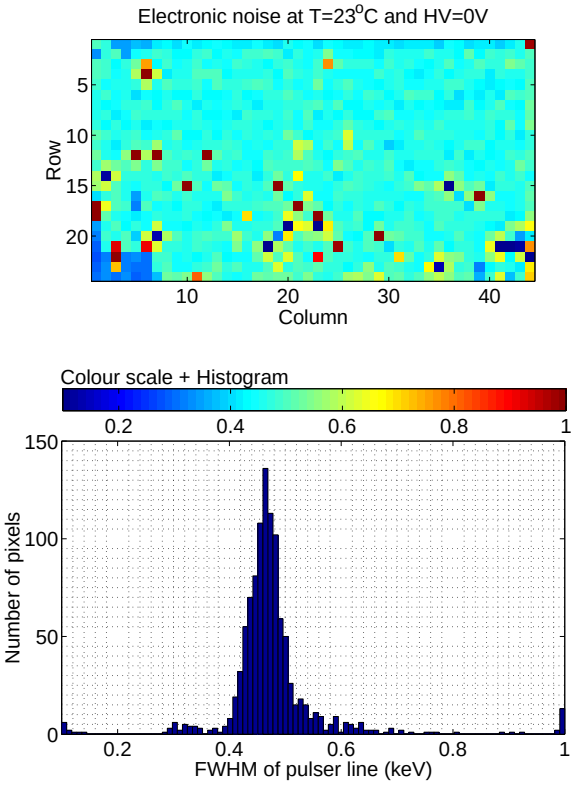

Fig. 4. Map and histogram of the electronic noise distribution at room temperature, with the voltage bias off. The pixels at the bottom-left corner are unconnected, and thus have lower noise amplitudes, between 0.3 and 0.4 keV FWHM. All anode contacts on Row 1 are narrower than the ones in the remaining rows; note the lower noise level across Row 1.

Figure 4 is a map of the electronic noise at each pixel at room temperature with the bias off. The blue spots represent quieter pixels, whereas the red spots represent noisier pixels. The same data is tallied here into a histogram, whose horizontal axis is aligned with the colour scale for the map. For our detector, the electronic noise amplitude is dominated by the input capacitance between the anode contacts on the CdZnTe and the ASIC backplane. So, unconnected pixels such as the ones at the bottom left corner of the map have lower noise amplitudes, as indicated in their positions in the histogram, between 300 and 400 eV. Also, the contacts are narrower in

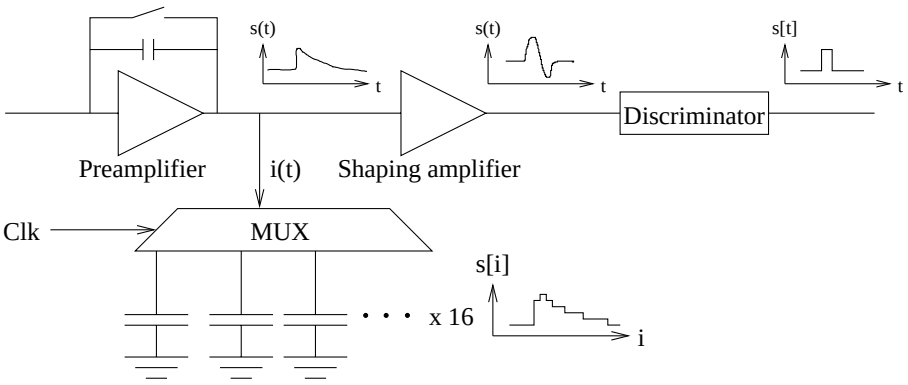

Fig. 3. Schematic diagramme of the HEFT ASIC read-out chip.

the row of pixels next to the mating edge of the detector. Here, the electronic noise amplitude is also smaller than the other pixels on the detector. On average, the electronic noise in our detector is between 400 and 600 eV at room temperature.

B. Leakage Current

Another property of interest is leakage current. Figure 5 shows the map and histogram of leakage current at each pixel, at room temperature; again, the redder pixels indicate higher leakage currents, while the bluer pixels indicates lower leakage currents. The map and histogram both show that there is substantial variation in the leakage current in this 12×22 mm^2 area of CdZnTe. However, if one cools the detector down to 0^oC, then the leakage current becomes negligible. We plot simple i-v curves at the two temperatures in Figure 6.

For practical reasons (to collect sufficient statistics in a reasonable time), we further study the performance of a subset of pixels with an X-ray source at 0^oC. Although the leakage current is negligible at this temperature, we have nevertheless chosen two regions of pixels with very different leakage characteristics at room temperature for further study, as this choice can potentially reveal further differences in material properties in the two regions. These two regions are indicated by the two circles in Figure 5.

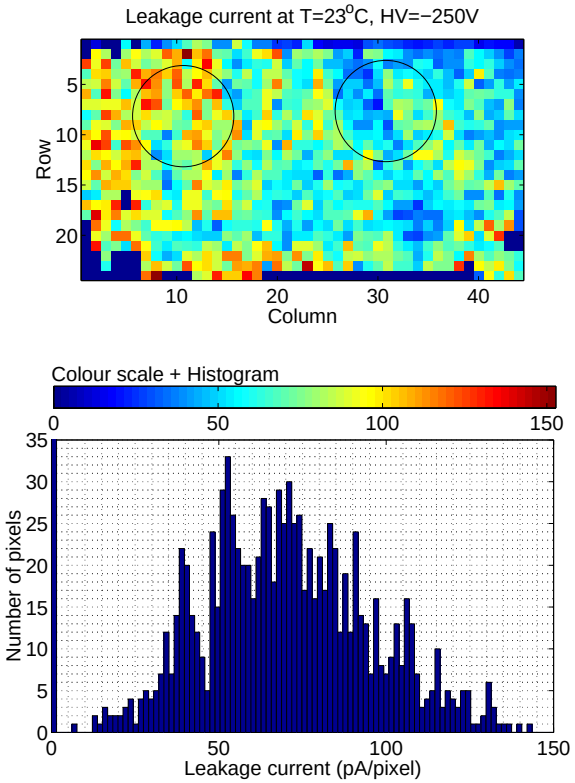

Fig. 5. Leakage current map and histogram at room temperature. There is substantial variation in the leakage current at room temperature, with strong spatial correlation. The circles indicate the two regions at which Am-241 spectra are obtained at 0^oC. The spectra are displayed in Figures 7 and 8.

C. Spectral Resolution

For each of the two regions selected, we illuminate it with an Am-241 source that is collimated to within a circle of about ten pixels in diameter. We then measure the spectrum at each region at 0^oC, which are shown in Figure 7 for the region with high leakage currents at room temperature, and in Figure 8 for the region with low leakage at room temperature. Both of these spectra include all events where one or two adjacent pixels are triggered (where one has to reconstruct the photon energy by adding the pulse heights from the two pixels together properly), and these events account for more than 90% of all the events. At low energies, the line widths are comparable to the size of the eletronic noise, which is the dominating factor. At high energies, the line width is further affected by variation in the depth of photon interaction, and the energy resolution is close to about 1 keV FWHM at 60 keV at 0^oC. As was indicated in the previous section, leakage current turns out not to be an issue at 0^oC.

D. Count Rate Uniformity

Yet another important property for a detector is the uniformity of count rate. We measure the count rate by illuminating the entire detector with an uncollimated point source, and measuring the number of counts at each pixel. Figure 9 shows

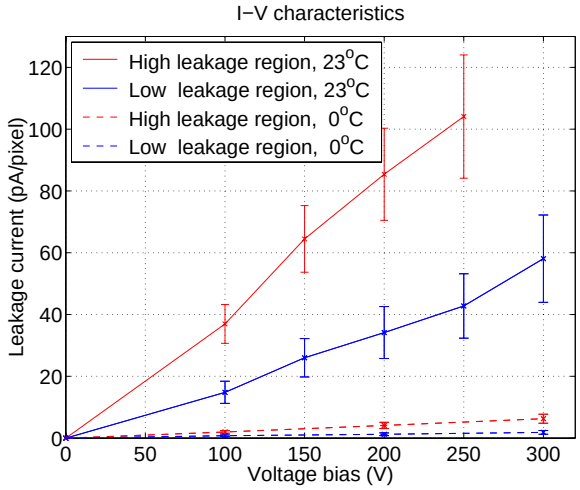

Fig. 6. Current-voltage relations for the two regions circled in Figure 5, at two different temperatures. There is substantial difference in the two regions at room temperature, but the leakage current becomes negligible at 0^oC.

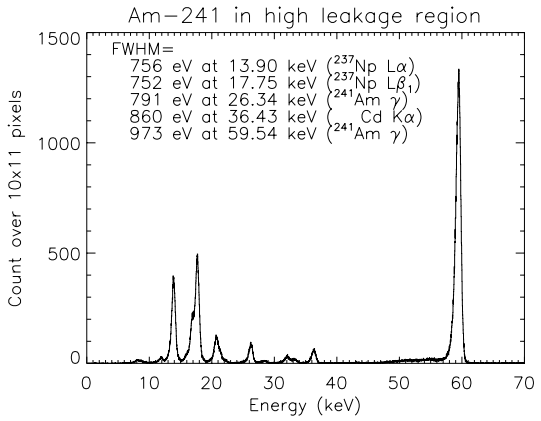

Fig. 7. Am-241 spectrum at 0^oC, obtained from the high-leakage region (at room temperature) circled in Figure 5. The cathode-to-anode potential is $HV = -400$ V.

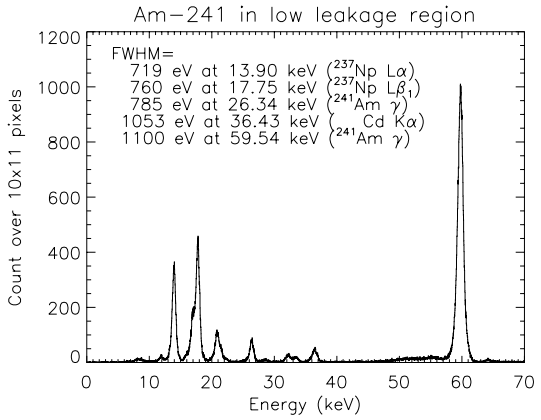

Fig. 8. Am-241 spectrum at 0^oC, obtained from the low-leakage region (at room temperature) circled in Figure 5. The cathode-to-anode potential is $HV = -400$ V.

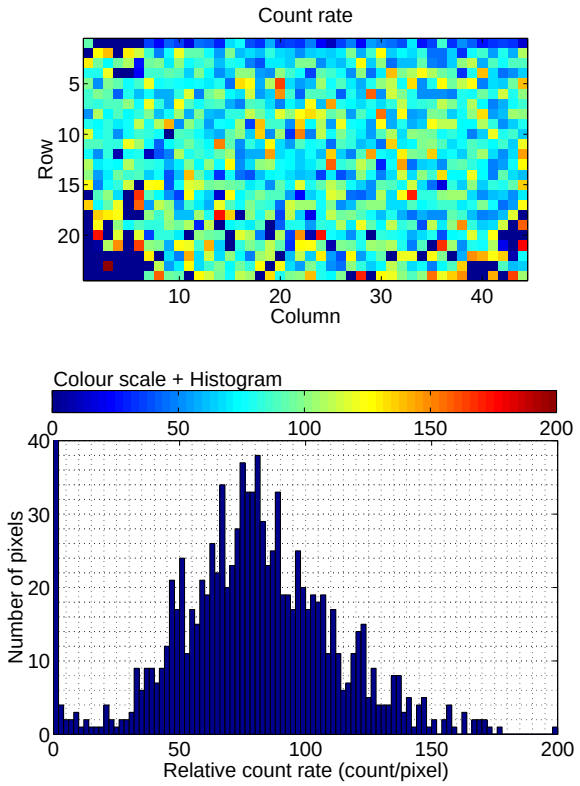

Fig. 9. Count rate map and histogram.

the map and histogram of the count rate; as this histogram indicates, we have observed high variation in the count rate that is clearly more than merely Poisson statistics, with the variation being close to the mean. On the positive side, these variations are stable, and thus correctable when the detector is put into use. However, we have tested an identical ASIC that is bonded to a cadmium telluride sensor instead of CdZnTe, and we have not seen such high count rate variation with the cadmium telluride detector. So, this variation in the count rate seems to be a CdZnTe property.

We suspect that this variation may be due to a non-uniform electric field within the CdZnTe, which causes each pixel to have a different 'effective collecting area'. If this is indeed the case, then a gain in collecting area by a pixel will be compensated by a corresponding loss of area by neighbouring pixels. So, if one averages the count rate at each pixel with the rates at its neighbours, the resulting distribution should be fairly uniform. This distribution is shown in Figure 10, where we convolve the rates in Figure 9 with a boxcar of three pixels in width in each direction. The distribution after this convolution agrees with Poisson statistics (mean=80.21 counts; 1σ=8.59 counts). Based on the same logic, one would expect to see a correlation between the count rate and the leakage current at each pixel. The correlation is plotted in Figure 11, and we do see some correlation.

We note that this investigation of the count rate is still under active investigation as of the writing of this paper; a scan of

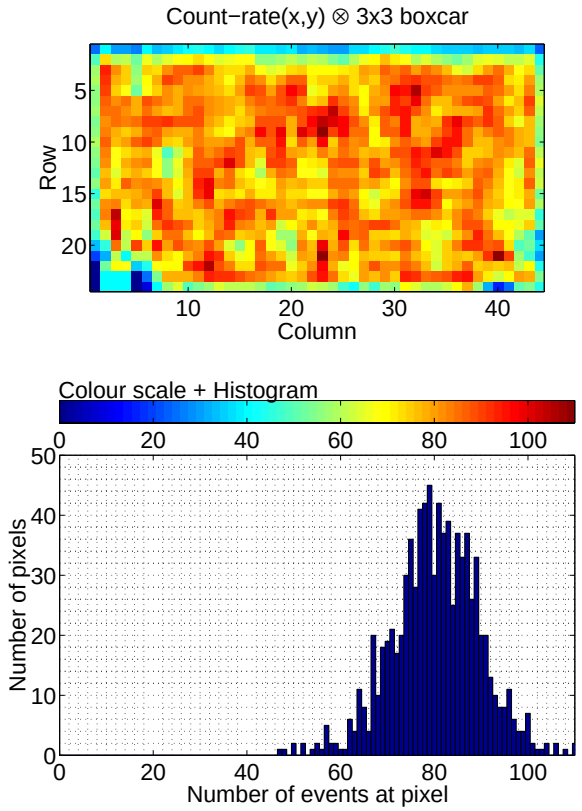

Fig. 10. Map and histogram of the count rate convolved with a boxcar of three pixels in width in each direction. Pixels on Row 1 have lengths that are 60% of the normal pitch; the count rates are thus lower accordingly. The lower rates on Row 2 and at the remaining three edges of the detector are due to the convolution of a finite data set. Pixels at the lower left corner are unconnected. Only pixels in $[2, 43] \times [3, 23] \backslash [2, 6] \times [20, 23]$ are included in the histogram. Mean=80.21 counts; 1σ=8.59 counts.

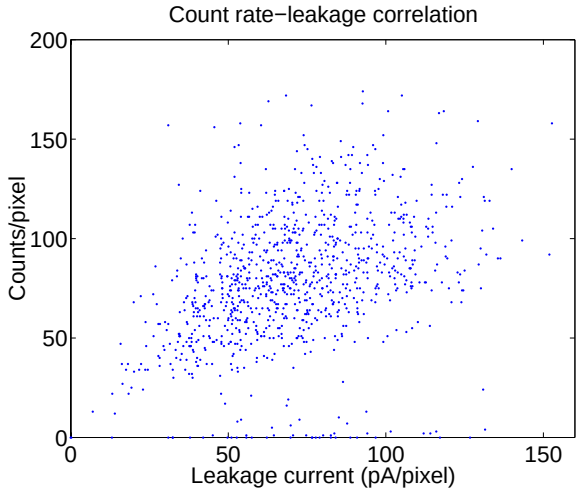

Fig. 11. Leakage current-count rate correlation for the HEFT detector.

TABLE I

SUMMARY OF SOME QUANTITATIVE PROPERTIES OF THE HEFT DETECTOR

Property	Range
Leakage current	10–140+ pA/pixel at 23^oC
	0–10 pA/pixel at 0^oC
Eletronic noise	400–600 eV FWHM at 23^oC, bias off
Spectral resolution	$\approx$ 1.0 keV FWHM at 60 keV at 0^oC
Count rate	variation $\approx$ mean

the detector with a fine X-ray beam and the calibration of the beam with a detector of known efficiency, both to be done in the near future, will provide us with more concrete information on the count rate.

IV. SUMMARY

In summary, for the High Energy Focusing Telescope, we have developed CdZnTe pixel detectors with large format, fine pitch and low power consumption. The leakage current varies substantially at room temperature, but is negligible at 0^oC. The electronic noise is around 500 eV at 23^oC, whereas the spectral resolution is about 1 keV FWHM at 60 keV at 0^oC. Table I summarizes the values of various quantities for the detector. We are still actively investigating the high variation in the count rate, and we shall report new results on this topic in a future paper.

ACKNOWLEDGEMENT

This research was supported by the NASA Space Science "Supporting Research and Technology" (SR&T) programme under Grant Number NAG5-5398. FAH was further supported by a Presidential Early Career Award, Grant Number NAG5-5322. JL was supported by the National Science Foundation under Grant Number DMR-020-4920. We are grateful for their support. Jill Burnham, Branislav Kecman and John Klemic have played crucial roles in the fabrication and testing of the detectors. CMHC thanks Dr Brian D. Ramsey for his suggestions during the conference.

REFERENCES

[1] F. A. Harrison, S. E. Boggs, A. E. Bolotnikov, F. E. Christensen, W. R. Cook, W. W. Craig, C. J. Hailey, M. A. Jimenez-Garate, P. H. Mao, S. M. Schindler, and D. L. Windt, "Development of the High-Energy Focusing Telescope (HEFT) balloon experiment," in *X-Ray Optics, Instruments, and Missions III*, ser. Proc. SPIE, J. E. Truemper and B. Aschenbach, Eds., vol. 4012, July 2000, pp. 693–699.

[2] F. A. Harrison, W. R. Cook, F. E. Christensen, O. Citterio, W. W. Craig, N. A. Gehrels, P. Gorenstein, J. E. Grindlay, C. J. Hailey, R. A. Kroeger, H. Kuneida, G. Pareschi, A. M. Parsons, R. Petre, and S. E. Romaine, "Technology development for the Constellation-X hard-x-ray telescope," in *EUV, X-Ray, and Gamma-Ray Instrumentation for Astronomy X*, ser. Proc. SPIE, O. H. Siegmund and K. A. Flanagan, Eds., vol. 3765, Oct. 1999, pp. 104–111.

[3] C. M. H. Chen, W. R. Cook, F. A. Harrison, J. Y. Y. Lin, P. H. Mao, and S. M. Schindler, "Characterization of the HEFT CdZnTe pixel detectors," in *Hard X-Ray and Gamma-Ray Detector Physics V*, ser. Proc. SPIE, L. A. Franks, A. Burger, R. B. James, and P. L. Hink, Eds., vol. 5198, in print.

[4] J. E. Clayton, C. M. H. Chen, W. R. Cook, and F. A. Harrison, "Assembly technique for a fine-pitch, low-noise interface; joining a CdZnTe pixel-array detector and custom VLSI chip with Au stud bumps and conductive epoxy," in *2003 IEEE Nuclear Science Symposium and Medical Imaging Conference Conference Record*, in print.